

Tidal interaction in compact binaries: a post-Newtonian affine framework

V. Ferrari, L. Gualtieri, A. Maselli

Dipartimento di Fisica, “Sapienza” Università di Roma & Sezione INFN Roma1, Piazzale Aldo Moro 5, 00185, Roma, Italy

We develop a semi-analytical approach, based on the post-Newtonian expansion and on the affine approximation, to model the tidal deformation of neutron stars in the coalescence of black hole-neutron star or neutron star-neutron star binaries. Our equations describe, in a unified framework, both the system orbital evolution, and the neutron star deformations. These are driven by the tidal tensor, which we expand at $1/c^3$ post-Newtonian order, including spin terms. We test the theoretical framework by simulating black hole-neutron star coalescence up to the onset of mass shedding, which we determine by comparing the shape of the star with the Roche lobe. We validate our approach by comparing our results with those of fully relativistic, numerical simulations.

PACS numbers: 04.25.Nx, 04.30.Dg, 04.25.dk

I. INTRODUCTION

Coalescing binaries composed of neutron stars (NS) and/or black holes (BH), are among the most promising sources of gravitational waves (GWs) to be detected by gravitational wave interferometers like Virgo and LIGO [1]. These systems are also interesting since they are thought to be related to short gamma-ray burst [2].

The process of coalescence has been studied mainly using post-Newtonian (PN) and fully relativistic, numerical simulations. PN expansion [3] has the advantage of providing a semi-analytic description of the evolution of the system, but it is poorly convergent in the strong field limit; therefore it is appropriate to study the inspiral phase only. These limitations have been overcome by PN resummed formulations like EOB [4], but these formulations are not able to describe the dynamical features of the stellar deformation. Moreover, in the standard PN expansion the compact objects are treated as pointlike up to the 4.5 (included) post-Newtonian order. Finite size effects are, formally, of order 5PN; however their contribution is larger than what a naive counting of PN orders may suggest [5]. Tidal deformations have recently been included in the PN framework through the “Love number” approach [6, 7], which assumes that the tidal field is proportional to the quadrupole momentum (see below). The effects of the tidal deformation on the orbital motion have been studied in [8, 9].

Fully relativistic codes are the most powerful tool to investigate the latest phases of the inspiral and merger (see [10] for a review on the subject). They are, however, not exempt from drawbacks: their computational cost is high, therefore the parameter space cannot be explored at large; furthermore, initial data solvers are still unable to provide accurate initial data for binaries with non-aligned spins, and may introduce spurious numerical effects which, if not appropriately cured, affect the subsequent evolution of the system. These problems are of particular relevance in BH-NS binaries, where the lack of symmetry makes more difficult to follow the entire process of coalescence by fully relativistic simulations. For these reasons, the process has been studied in the liter-

ature using some simplifying assumptions, or for a restricted set of parameters. For instance, in [11–14] the inspiral is modeled as a sequence of quasi-equilibrium circular orbits with decreasing radius; in [11, 12] the process is studied by fully relativistic simulations, whereas [13, 14] use the affine approach (see below). In [15, 16] Einstein’s equations are evolved assuming that the black hole is non rotating, and for large values of the mass ratio $q = M_{BH}/M_{NS}$, whereas in [17–20] q takes values $q \leq 5$; in [20, 21] the black hole is assumed to rotate with spin parallel to the orbital angular momentum, and different values have been considered. For a recent review on fully relativistic simulations of BH-NS binaries see [22] (the literature on NS-NS coalescing binaries is much more extended, and we do not report it here).

In this paper we develop a semi-analytic approach to study BH-NS and NS-NS coalescence, by merging two different frameworks: the PN approach, which accurately describes the system orbital motion, and the affine model [13, 14, 23–26], which describes the stellar deformations induced by the tidal field. To this aim, we compute the tidal tensor associated to the PN metric of a two-body system, defined in terms of the PN Riemann tensor and of the local tetrad of the deformed body

$$C_{(i)(j)} = R_{\alpha\beta\gamma\delta} e_{(0)}^\alpha e_{(i)}^\beta e_{(0)}^\gamma e_{(j)}^\delta, \quad (1)$$

up to $O(1/c^3)$. This tensor was derived with a different approach in [27–29] up to $O(1/c^2)$; our expression coincides with that of [29] and also includes $O(1/c^3)$ terms, associated to the spins of the compact objects.

In the affine model the NS is described as a deformable ellipsoid, subject to its self-gravity, to internal pressure forces and to the tidal field of the companion. In the original formulation of this approach, the NS structure was considered at a Newtonian order, assuming a polytropic equation of state (EOS) [23–26]. A first improvement was introduced in [13, 14], where general relativity was taken into account in the description of the stellar structure, and non-polytropic EOSs were considered. This approach was used to study quasi-equilibrium configuration sequences of BH-NS systems, in order to estimate the critical distance at which the NS is disrupted by

the tidal interaction [13], to determine the corresponding cut-off frequency in the emitted gravitational wave signal [14, 30], and to estimate the mass of the torus which forms after the NS is disrupted [31].

In this paper we further improve the affine model introducing a more accurate description of the orbital motion and of the tidal interaction. Our approach differs from existing work on NS tidal deformation in compact binaries in the following aspects.

- In [13, 14, 25, 26, 31, 32] the affine model was used assuming that the NS follows a timelike geodesic of Kerr’s spacetime; this approximation fails when the mass ratio q is low. In addition, time-dilation factors were neglected.

Furthermore, most works employing the affine model [13, 14, 25, 26] do not evolve the dynamical equations of stellar deformation. Rather, they find, at each value of the orbital radius, the corresponding stationary configuration describing the deformed star. In [31, 32] the dynamical equations were solved; however, while the orbital evolution was described in PN coordinates, the BH tidal field was expressed in the Boyer-Lindquist coordinates of the Kerr metric describing a single BH; neglecting the difference between these coordinate systems yields a loss of accuracy of the model.

These problems are solved in the fully consistent approach presented in this paper, where the BH-NS or NS-NS systems are described by a two-body PN metric, *which holds for any value of the mass-ratio q* . The tidal tensor itself is expressed in the PN coordinates, and the proper time of each compact body is expressed in terms of the PN time coordinate, through the appropriate Lorentz factor. Our approach is valid up to the onset of mass shedding, which occurs when the deformed star crosses the Roche lobe; after that, it can no longer be applied, since the assumption that the star is a deformed ellipsoid is significantly violated. We describe the orbital motion of the compact objects using the 3.5 PN equations for pointlike objects, with next-to-leading-order tidal corrections; the NS tidal deformation is driven by the tidal tensor of the 3 PN metric. The dynamical equations are a system of (non-linear) ordinary differential equations in time.

- NS tidal deformations have also been studied in a series of paper [6, 7, 33–36], where the deformation properties have been encoded in a set of numbers, the *Love numbers*, which relate the quadrupole tensor (or, more generally, the multipole moments of the star) to the tidal tensor. This approach is grounded on the *adiabatic approximation*, i.e., on the assumption that the orbital evolution timescale is much larger than the timescale needed for the star to set into a stationary configuration. In this approximation, the quadrupole tensor is propor-

tional to the tidal tensor:

$$Q_{(i)(j)} = \lambda C_{(i)(j)}, \quad (2)$$

with λ constant. The Love number λ can be computed by studying the response of a single star to an external tidal tensor [6, 7, 34, 35]. This model has been employed to determine the effect of tidal deformation on the orbital motion of a NS in a binary system [8, 29, 33, 36].

We also compute the Love number λ (see Section III), without assuming the adiabatic approximation: the stellar deformation is found by solving dynamical equations.

To test the accuracy of our approach, we compare the results with the existing literature on BH-NS binaries. As a preliminary check, we verify that our PN description of the orbital motion accurately reproduces the fully relativistic results [18, 20, 37]. Then, we verify that the onset of mass shedding we determine, is consistent with the results of fully relativistic simulations [18, 20, 37]. Finally, we check that the stellar deformations predicted by our model are consistent with existing computations of the Love number [6, 7, 34, 35].

This paper focuses mainly on the theoretical framework, and on its validation by comparison with the existing literature, where available. The tool we develop will be used in future works to study the dynamics of compact binaries.

The plan of the paper is the following. In Sec II we describe the model. In Sec. III we assess the validity of our approach, by comparing the results with the literature. In Sec. IV we draw the conclusions.

II. THE MODEL

We use notations and conventions introduced in [13], where the affine model (partially improved with respect to the original formulation [23, 24]) is widely discussed. In the following m_1, m_2 are the masses of the two compact objects; we shall consider the tidal deformation of the NS with mass m_1 and radius R_{NS} ; the companion, with mass m_2 , can either be a BH or a NS. Furthermore, we define $m = m_1 + m_2$ and $\nu = \mu/m = m_1 m_2 / m^2$, and the mass ratio $q = m_2 / m_1$.

A. Improved affine model

The basic assumption of the affine model is that the NS, deformed by the tidal field, maintain an ellipsoidal shape; it is an *S*-type Riemann ellipsoid, i.e., its spin and vorticity are parallel, and their ratio is constant [38]. The deformation equations are written in the *star principal frame*, i.e., the frame comoving with the star, whose axes coincide with the ellipsoid principal axes. In what

follows, a_1 is the axis which points toward the companion; a_2 and a_3 are the axes orthogonal to a_1 , with a_2 lying in the orbital plane; the indices 1,2,3 label the corresponding directions. Surfaces of constant density inside the star form self-similar ellipsoids and the velocity of a fluid element is a linear function of the coordinates x^i in the principal frame. Under these assumptions, the infinite degrees of freedom of the stellar fluid motion can be reduced to five [23–25], and are associated to dynamical variables governed by a set of non-linear differential equations, which describe the evolution of the stellar deformation. These variables are the three principal axes of the ellipsoid a_i ($i = 1, 2, 3$) and two angles, ψ , λ , defined as

$$\frac{d\psi}{d\tau} = \Omega, \quad \frac{d\lambda}{d\tau} = \Lambda, \quad (3)$$

where τ is the NS proper time, and Ω is the ellipsoid angular velocity, measured in the parallel transported frame associated with the star center of mass. ψ is the angle between the principal frame and the parallel transported frame. Λ is defined as follows:

$$\Lambda = \frac{a_1 a_2}{a_1^2 + a_2^2} \zeta, \quad (4)$$

where ζ is the vorticity along the axis x^3 in the principal frame. The NS internal dynamics is described in terms of the Lagrangian

$$\mathcal{L}_I = T_I - U - \mathcal{V}, \quad (5)$$

where T_I is the fluid kinetic energy, U is the internal energy and \mathcal{V} is the star self-gravity. In the original approach introduced by Carter and Luminet, these are defined in a Newtonian framework

$$T_I = \frac{1}{2} \int v^2 dM_B, \quad (6)$$

$$U = \int \frac{\epsilon}{\rho} dM_B, \quad (7)$$

$$\mathcal{V} = -\frac{G}{2} \int \frac{dM_B dM'_B}{|\mathbf{x} - \mathbf{x}'|} = \int dM_B r \partial_r \Phi_{Newt}, \quad (8)$$

where M_B is the baryonic mass, ρ the mass density, ϵ the Newtonian energy density, Φ_{Newt} the gravitational potential; all these quantities are solutions of the Newtonian equations of stellar structure. Furthermore, $dM_B = \rho d^3x$ and \mathcal{V} satisfies the virial theorem, which states that, in the spherical configuration, $\mathcal{V} = -3\Pi$, where

$$\Pi = \int \frac{p}{\rho} dM_B = \int p d^3x. \quad (9)$$

The variation of the Lagrangian (5) gives the equations of motion for the five dynamical variables a_i , ψ , λ .

In [23, 24] it was shown that, under the affine hypothesis, the integrals in Eqns. (6-8) and their variations, can be expressed in terms of integrals on the fluid variables computed for the spherical configuration ($a_i = R_{NS}$),

and of functions of the dynamical variables. With this simplification, the equations of motion can easily be found. In the following, a superscript hat will denote quantities computed for the spherical star. T and \mathcal{V} expressed in terms of the “hatted” quantities and of the dynamical variables are

$$T_I = \sum_i \frac{1}{2} \left(\frac{da_i}{d\tau} \right)^2 \frac{\hat{\mathcal{M}}}{R_{NS}^2} + \frac{1}{2} \frac{\hat{\mathcal{M}}}{R_{NS}^2} \left[\left(\frac{a_1}{a_2} \Lambda - \Omega \right)^2 a_2^2 + \left(\Omega - \frac{a_2}{a_1} \Lambda \right)^2 a_1^2 \right] \quad (10)$$

$$\mathcal{V} = \frac{1}{2} \hat{\mathcal{V}} R_{NS} \int_0^\infty \frac{d\sigma}{\sqrt{(a_1^2 + \sigma)(a_2^2 + \sigma)(a_3^2 + \sigma)}}, \quad (11)$$

where $\hat{\mathcal{M}}$ is the *scalar quadrupole moment*

$$\hat{\mathcal{M}} = \frac{1}{3} \int_{sph} \sum_i (x_i)^2 dM_B \quad (12)$$

(the subscript *sph* means that the integration is performed on the spherical star) and $\hat{\mathcal{V}}$ is the self-gravity potential of the spherical star.

The procedure to make explicit the dependence of the internal energy U on the dynamical variables is more subtle. The internal energy variation dU can be written as

$$dU = \sum_i \frac{\Pi}{a_i} da_i. \quad (13)$$

The pressure integral Π given by Eq. (9) can not be factorized in a spherical integral and a function of the axes; however, it can be expressed as

$$\Pi = \frac{a_1 a_2 a_3}{R_{NS}^3} \int_{sph} p(\rho) d^3x, \quad (14)$$

where $p(\rho)$ is the fluid equation of state, and ρ is the rescaled mass density

$$\rho = \hat{\rho} \frac{R_{NS}^3}{a_1 a_2 a_3} \quad (15)$$

with $\hat{\rho}$ mass density in the spherical configuration. When $a_i = R_{NS}$, the pressure integral Π reduces to the spherical pressure integral $\hat{\Pi}$.

A first improvement to this approach was introduced in [13], where the Newtonian description of the NS equilibrium configuration was replaced by the relativistic equations of stellar structure (TOV)

$$\partial_{r_s} m_s = 4\pi \hat{e} r_s^2$$

$$\partial_{r_s} \hat{p} = -G \frac{(\hat{e} + \hat{p}/c^2)(m_s + 4\pi \hat{p} r_s^3/c^2)}{r_s(r_s - 2Gm_s/c^2)}. \quad (16)$$

Here \hat{e} is the relativistic mass-energy density in the spherical configuration, r_s is the radial coordinate in a Schwarzschild frame associated to the non rotating NS, and $m_s(r_s)$ is the gravitational mass enclosed in a sphere

of radius r_s . We remark that this is a major change, since the relativistic radius is smaller than the Newtonian radius by $\sim 10\% - 20\%$. We also remark that the Schwarzschild coordinate r_s is different from the radial coordinate in the Newtonian frame $r = \sum_i (x_i^2)^{1/2}$. The self-gravity integral \hat{V} was changed accordingly, as

$$\hat{V} = \int_{sph} dM_B r_s \partial_{r_s} \Phi_{TOV}, \quad (17)$$

where Φ_{TOV} is an effective relativistic gravitational potential of the spherical star, defined in terms of the TOV equations as follows

$$\hat{\rho} \partial_{r_s} \Phi_{TOV} = G \frac{(\hat{\epsilon} + \hat{p}/c^2)(m_s + 4\pi r_s^3 \hat{p}/c^2)}{r_s(r_s - 2Gm_s/c^2)}. \quad (18)$$

With this definition the virial theorem

$$\int_{sph} r_s \partial_{r_s} \Phi_{TOV} dM_B = -3 \int_{sph} \frac{\hat{p}}{\hat{\rho}} dM_B \quad (19)$$

is still satisfied, with \hat{p} solution of the TOV equations (16) and $\hat{\rho}$ baryon mass density. As shown in Section II E, some terms in the dynamical equations cancel in the spherical limit, only if the virial theorem is satisfied. A non-exact cancellation of these terms would lead to strong instabilities.

A further improvement, which we introduce in this paper, consists in a careful treatment of the coordinate frames. To describe the integrals in the spherical configuration, the relevant coordinate systems are: (i) the Schwarzschild frame, with radial coordinate r_s , in which the TOV equations (16) are expressed; (ii) the Newtonian frame for a spherical star $\{x^i\}$, which we now replace with the corresponding 1 PN post-Newtonian frame [3], with isotropic radial coordinate $r = \sum_i (x_i^2)^{1/2}$ and metric (for a single star)

$$ds^2 = - \left(1 - \frac{2V}{c^2} + \frac{2V^2}{c^4} \right) dt^2 + \left(1 + \frac{2V}{c^2} \right) \delta_{ij} dx^i dx^j, \quad (20)$$

where $V(r) \equiv G \int_r^\infty \frac{m_s(r')}{r'^2} dr'$. Following [39] the transformation between the post-Newtonian isotropic radial coordinate and the Schwarzschild coordinate inside the star is given by

$$r = r_s \left(1 - \frac{V(r_s)}{c^2} \right). \quad (21)$$

The scalar quantity dM_B can be expressed, in the Schwarzschild frame, in terms of the corresponding spatial three-metric γ_{schw}^{ij} :

$$\begin{aligned} dM_B &= \hat{\rho} \sqrt{\gamma_{schw}} d^3x \\ &= \hat{\rho} r_s^2 \left(1 + \frac{Gm_s(r_s)}{r_s c^2} \right) dr_s \sin \theta d\theta d\phi. \end{aligned} \quad (22)$$

The integrand in the quadrupole moment (12) is expressed in the post-Newtonian coordinates, i.e., it is $r^2 = r_s^2(1 - 2V(r_s)/c^2)$. The integrals \hat{V} , $\hat{\Pi}$, $\hat{\mathcal{M}}$ then take the form

$$\begin{aligned} \hat{V} &= -3\hat{\Pi} \\ \hat{\Pi} &= 4\pi \int_0^{R_{NS}} \hat{p} \left(1 + \frac{Gm_s(r_s)}{r_s c^2} \right) r_s^2 dr_s \\ \hat{\mathcal{M}} &= \frac{4\pi}{3} \int_0^{R_{NS}} \hat{\rho} \left(1 - \frac{2V(r_s)}{c^2} + \frac{Gm_s(r_s)}{r_s c^2} \right) r_s^4 dr_s. \end{aligned} \quad (23)$$

B. The post-Newtonian metric

To derive the equations describing the orbital motion of the binary and the tidal tensor, we shall use a 3 PN metric written in harmonic coordinates ($\{x^\mu = ct, x, y, z\}$):

$$g_{00} = -1 + \frac{2V}{c^2} - \frac{2V^2}{c^4} + \frac{8}{c^6} \left[\hat{X} + V_i V_i + \frac{V}{6} \right] + \frac{32}{c^8} \left[\hat{T} - \frac{V\hat{X}}{2} + \hat{R}_i V_i - \frac{VV_i V_i}{2} - \frac{V^4}{48} \right] + \mathcal{O}(10) \quad (24)$$

$$g_{0i} = -\frac{4}{c^3} V_i - \frac{8}{c^5} \hat{R}_i - \frac{16}{c^7} \left[\hat{Y}_i + \frac{1}{2} \hat{W}_{ij} V_j + \frac{1}{2} V^2 V_i \right] + \mathcal{O}(9) \quad (25)$$

$$g_{ij} = \delta_{ij} \left[1 + \frac{2}{c^2} V + \frac{2}{c^4} V^2 + \frac{8}{c^6} \left(\hat{X} + V_k V_k + \frac{V^3}{6} \right) \right] + \frac{4}{c^4} \hat{W}_{ij} + \frac{16}{c^6} \left(\hat{Z}_{ij} + \frac{1}{2} V \hat{W}_{ij} - V_i V_j \right) + \mathcal{O}(8), \quad (26)$$

where the potentials $V, V_i, \hat{X}, \hat{W}_{ij}, \hat{R}_i, \hat{Y}_i, \hat{Z}_{ij}$, are defined in terms of retarded integrals over the source densities [40, 41]. We stress that the potential V appearing in

the metric of the two-body system (24)-(26), is different from the potential V in Eq. (20), which is the metric of a single star. Since these potentials are written as

expansions of powers of $1/c^n$, in the following we shall identify the order of expansion with a superscript index. Thus, $V^{(0)}$ defines the scalar potential of order 0 in $1/c$, $V^{(2)}$ is the $1/c^2$ term and so on.

C. The orbital motion

Following [42], we assume that the orbit evolves as a slow adiabatic inspiral of a quasi-circular orbit, i.e., the energy lost through gravitational waves is balanced by a change of the total binding energy E of the system

$$\frac{dE}{dt} = -\mathcal{F}, \quad (27)$$

where E and the GW flux \mathcal{F} are expressed in terms of the PN variable

$$x = \left(\frac{Gm\omega}{c^3}\right)^{2/3}, \quad (28)$$

being $\omega = d\phi/dt$ the orbital frequency. Eq.(27) yields

$$\frac{dx}{dt} = -\frac{\mathcal{F}}{dE/dx}. \quad (29)$$

We neglect the orbital eccentricity because, due to gravitational wave emission, the orbit circularizes well before the latest stages of the inspiral which we are studying [43]. We use the approach named ‘‘Taylor T4 approximant’’ [44, 45], in which the right-hand side of eq.(29) is expanded to 3.5 PN order including spin terms. We also include the effects of the NS tidal deformation on the orbital motion, up to next-to-leading-order [8]. The orbital phase $\phi(t)$ and the orbital frequency ω are computed by numerically integrating the following ODEs

$$\frac{dx}{dt} = \frac{dx}{dt}\Big|_{pp} + \frac{dx}{dt}\Big|_{tidal} \quad (30)$$

$$\frac{d\phi}{dt} = \frac{c^3}{Gm} x^{3/2}. \quad (31)$$

where the point-particle contribution reads

$$\frac{dx}{dt}\Big|_{pp} = \frac{64}{5} \frac{\nu}{m} x^5 \sum_{k=0}^7 a_k x^{k/2} \quad (32)$$

with the coefficient a_k given in Appendix A, and the tidal term is given by

$$\begin{aligned} \frac{dx}{dt}\Big|_{tidal} = & \frac{32m_1\lambda_2}{5m^7} \left\{ 12 \left[1 + 11 \frac{m_1}{m} \right] x^{10} + \left[\frac{4421}{28} - \frac{12263}{28} \frac{m_2}{m} \right. \right. \\ & \left. \left. + \frac{1893}{2} \frac{m_2^2}{m^2} - 661 \frac{m_2^3}{m^3} \right] x^{11} \right\} + 1 \leftrightarrow 2, \end{aligned} \quad (33)$$

where λ_2 is the Love number of the body 2, and $1 \leftrightarrow 2$ means the same terms but with the label 1 and 2 exchanged. As we discuss in Section III B, the values of the Love number for different stellar models can be computed

with our approach, and agree with the values obtained in the literature [7].

The orbital separation r_{12} is evaluated through the PN expression for $\gamma = Gm/r_{12}c^2$, which is known up to order 3 PN, including spin terms [47], and is found solving the equation

$$\begin{aligned} \frac{d\gamma}{dt} = \frac{dx}{dt} & \left\{ 1 + 2x \left(1 - \frac{\nu}{3} \right) + \frac{5}{2} x^{3/2} \left(\frac{5}{3} s_\ell + \delta\sigma_\ell \right) + \right. \\ & + 3x^2 \left(1 - \frac{65}{12}\nu \right) + \frac{7}{2} x^{5/2} \left[\left(\frac{10}{3} + \frac{8}{9}\nu \right) s_\ell + \right. \\ & + 2\delta\sigma_\ell \left. \right] + 4x^3 \left[1 + \left(-\frac{2203}{2520} - \frac{41}{192}\pi^2 \right) \nu + \right. \\ & \left. \left. + \frac{229}{36}\nu^2 + \frac{\nu^2}{81} \right] \right\}, \end{aligned} \quad (34)$$

where $\delta = \frac{m_1 - m_2}{m}$ and the spin variables are defined as follows

$$s_\ell = \frac{c}{G} \frac{\mathbf{S}}{m^2} = \frac{c}{G} \frac{\mathbf{S}_1 + \mathbf{S}_2}{m^2} \quad (35)$$

$$\sigma_\ell = \frac{c}{G} \frac{\boldsymbol{\Sigma}}{m^2} = \frac{c}{Gm} \left[\frac{\mathbf{S}_2}{m_2} - \frac{\mathbf{S}_1}{m_1} \right]; \quad (36)$$

$\mathbf{S}_i = (G/c)m_i^2 \tilde{a}_i \hat{\mathbf{s}}_i$ are the spin angular momenta of bodies $i = 1, 2$, with dimensionless spin parameters \tilde{a}_i and unit direction vectors $\hat{\mathbf{s}}_i$.

It is important to remark that the adiabatic inspiral of the orbital motion and the ‘‘adiabatic approximation’’ for the Love number, are two different approximations: the first assumes that the orbital timescale is much larger than that associated to the gravitational wave energy loss (*orbital adiabatic approximation*); the second assumes, as mentioned in the Introduction and in Section III B, that the orbital timescale is much larger than the timescale associated to the NS internal dynamics (*Love number adiabatic approximation*). In this paper, we use the orbital adiabatic approximation, but we drop the Love number adiabatic approximation.

D. Post-Newtonian tidal deformations

Tidal interactions in binary systems have been studied by many authors in the framework of general relativity (see for instance [48, 49]). They are described by the equation of geodesic deviation:

$$\frac{D^2 \xi^\alpha}{D\tau^2} + R^\alpha_{\beta\gamma\delta} u^\beta u^\gamma \xi^\delta = 0, \quad (37)$$

where $R^\alpha_{\beta\gamma\delta}$ is the Riemann tensor, $D/D\tau = u^\mu \nabla_\mu$, and, in the present case, u^β is the 4-velocity of the star center O^* and ξ^α is the separation 4-vector between O^* and a generic fluid element. By introducing an orthonormal tetrad field $\{e^\mu_{(i)}\}$ ($i = 0, \dots, 3$) associated with the frame centered in O^* , parallel transported along its motion, and

such that $e_{(0)}^\mu = u^\mu$, Eq. (37) can be cast in the form [50]

$$\frac{d^2 \xi^{(i)}}{d\tau^2} + C_{(j)}^{(i)} \xi^{(j)} = 0, \quad (38)$$

where the $\xi^{(i)} = e_\mu^{(i)} \xi^\mu$, and $C_{(j)}^{(i)}$ are the components of the relativistic tidal tensor, defined in Eq. (1). In the affine approach, Eq. (38) applies with $\xi^{(i)}$ replaced by a_i .

In the following subsections, starting from the 3 PN metric given in Eqns. (24)-(26), we write the explicit expression of the parallel transported tetrad, and compute the tidal tensor assuming equatorial motion.

1. The parallel transported tetrad

The orthonormal tetrad associated to the PN metric (24)-(26), satisfies the Fermi-Walker transport equations (expressed in terms of the coordinate time t , rather than of the proper time of O^*) [51]:

$$\frac{de_{(\alpha)}^\mu}{dt} = \Pi_\nu^\mu e_{(\alpha)}^\nu, \quad (39)$$

where

$$\Pi_\nu^\mu = -\Gamma_{\nu\lambda}^\mu v^\lambda - \frac{1}{c^2} g_{\nu\lambda} (a^\mu v^\lambda - a^\lambda v^\mu), \quad (40)$$

a^μ is the 4-acceleration of O^* and $v^\mu = dx^\mu/dt$, $\mu = 0, 3$ its coordinate velocity, with $v^0 = c$. The tetrad vectors are [51]:

$$\begin{aligned} e_{(t)}^t &= \tilde{e}_{(t)}^t \\ e_{(t)}^j &= \tilde{e}_{(t)}^j \\ e_{(j)}^t &= \tilde{e}_{(j)}^t \\ e_{(x)}^j &= \cos \chi \tilde{e}_{(x)}^j + \sin \chi \tilde{e}_{(y)}^j \\ e_{(y)}^j &= -\sin \chi \tilde{e}_{(x)}^j + \cos \chi \tilde{e}_{(y)}^j \end{aligned}$$

$$e_{(z)}^j = \tilde{e}_{(z)}^j$$

where

$$\tilde{e}_{(t)}^t = 1 + \frac{1}{c^2} \left[V + \frac{v^2}{2} \right] + \mathcal{O}(4) \quad (41)$$

$$\tilde{e}_{(t)}^j = \frac{v^j}{c} + \left[V + \frac{v^2}{2} \right] \frac{v^j}{c^3} + \mathcal{O}(5)$$

$$\tilde{e}_{(j)}^t = \frac{v^j}{c} + \mathcal{O}(3)$$

$$\tilde{e}_{(k)}^j = \delta_k^j \left[1 - \frac{V}{c^2} \right] + \frac{v^j v^k}{2c^2} + \mathcal{O}(4),$$

and

$$\chi = \frac{1}{c^2} Q_{xy} \quad (42)$$

is the angle describing geodesic precession and frame dragging, given in terms of the antisymmetric matrix \mathbf{Q} defined as

$$\mathbf{Q}(t, t_0) = \int_{t_0}^t [\mathbf{v} \times (\nabla V - \mathbf{a}) - \nabla \times (V \mathbf{v} - 2\mathbf{V})] dt. \quad (43)$$

$\mathbf{V} = \{V_i\}$ is the post Newtonian potential, associated with the components g_{0i} of the PN metric (25), and t_0 is an arbitrary integration constant.

Eqns. (41) reduce to those given in ref. [51] with the identification $V^2 = -\psi$, $\gamma \delta_{ij} V = \chi_{ij}$ and $V_i = -\frac{1}{4} g_i$.

2. The tidal tensor

Having defined the tetrad field, we have explicitly computed (with the help of the symbolic manipulation software `maple` and the package `GRTensor`) the Riemann and the tidal tensors, up to order $1/c^3$. The general structure of the tidal tensor components in terms of the derivatives of the PN potentials, is given in Appendix B; here we show, as an example, the component $C_{(x)(x)}$:

$$\begin{aligned} C_{(x)(x)} &= -\partial_{xx}^2 V^{(0)} + \frac{1}{c^2} \left\{ -4\partial_{xt}^2 V_x^{(0)} + 4v^y \partial_{xx}^2 V_y^{(0)} - 4v^y \partial_{xy}^2 V_x^{(0)} - (\partial_y V^{(0)})^2 - \partial_{xx}^2 V^{(2)} - \left[\partial_{tt}^2 + (v^y)^2 (\partial_{yy}^2 + 2\partial_{xx}^2) + \right. \right. \\ &\quad \left. \left. + 2v^y \partial_{yt}^2 - v^x v^y \partial_{xy}^2 \right] V^{(0)} + 2\partial_{xx}^2 V^{(0)} V^{(0)} + 2(\partial_x V^{(0)})^2 \right\} - \frac{4}{c^3} \left\{ (\partial_{xt}^2 + v^y \partial_{xy}^2) V_x^{(1)} - v^y \partial_{xx}^2 V_y^{(1)} + \frac{1}{4} \partial_{xx}^2 V^{(3)} \right\} \quad (44) \end{aligned}$$

where [40, 41]

$$V^{(0)} = \frac{Gm_1}{r_1} + 1 \leftrightarrow 2 \quad (45)$$

$$V^{(2)} = Gm_1 \left[Gm_2 \left(-\frac{r_1}{4r_{12}^3} - \frac{5}{4r_1 r_{12}} + \frac{r_2^2}{4r_1 r_{12}^3} \right) + \right.$$

$$\left. - \frac{(\mathbf{n}_1 \cdot \mathbf{v}_1)^2}{2r_1} + \frac{2v_1^2}{r_1} \right] + 1 \leftrightarrow 2$$

$$V^{(3)} = -2G\epsilon_{ijk} v_1^i S_1^j \partial_k \left(\frac{1}{r_1} \right) + 1 \leftrightarrow 2$$

$$V_i^{(0)} = \frac{Gm_1 v_1^i}{r_1} + 1 \leftrightarrow 2$$

$$V_i^{(1)} = -\frac{G}{2} \epsilon_{ijk} S_1^j \partial_k \left(\frac{1}{r_1} \right) + 1 \leftrightarrow 2.$$

To hereafter we omit the parentheses to indicate the tetrad components of the tidal tensor. In Eqns. (45) $1 \leftrightarrow 2$ means the same term but with the labels 1 and 2 exchanged; $r_1 = |\mathbf{x} - \mathbf{y}_1|$ and $\mathbf{n}_1 = (\mathbf{x} - \mathbf{y}_1)/r_1$, where \mathbf{x} is the field point and $\mathbf{y}_1(t)$ the trajectory of m_1 (and similarly for m_2); $\mathbf{v}_1 = d\mathbf{y}_1(t)/dt$ is the coordinate velocity, $\mathbf{r}_{12} = \mathbf{r}_1 - \mathbf{r}_2$ the relative displacement between the two masses, and $\mathbf{v}_{12} = \mathbf{v}_1 - \mathbf{v}_2$ the relative velocity. ϵ_{ijk} is the 3-dimensional antisymmetric Levi-Civita symbol with $\epsilon_{123} = 1$, and S_1^j is the spin-vector.

The steps needed to evaluate the tidal tensor at the center of the NS (i.e., at location 1 in our conventions) are the following:

1. estimate the various derivatives of the PN potentials V, V_i ;
2. compute the tidal tensor at the source location $[C_j^i]_1 = C_j^i(\mathbf{x} \rightarrow \mathbf{y}_1)$, and apply a regularization procedure;
3. express all quantities in the two-body center of mass frame;
4. switch to the star principal frame defined in Section II A.

The second point requires further clarifications. Since the PN metric refers to pointlike sources, the PN potentials (45) diverge when computed at the source locations $\mathbf{x} \rightarrow \mathbf{y}_1$ and $\mathbf{x} \rightarrow \mathbf{y}_2$. To remove this divergence, we apply the Hadamard regularization procedure [40], which we briefly describe. Let $F(\mathbf{x}, \mathbf{y}_1, \mathbf{y}_2)$ be a function depending on the field point \mathbf{x} and on the two source locations $\mathbf{y}_1, \mathbf{y}_2$, and admitting, when \mathbf{x} approaches \mathbf{y}_1 , an expansion of the

form

$$F(\mathbf{x}, \mathbf{y}_1, \mathbf{y}_2) = \sum_k r_1^k f_k(\mathbf{n}_1, \mathbf{y}_1, \mathbf{y}_2) \quad k \in \mathbb{Z}. \quad (46)$$

The regularized value of F at the point 1 is the *Hadamard part finie*, which is the average, with respect to the direction \mathbf{n}_1 , of the $k = 0$ term in the sum (46):

$$(F)_1 = F(\mathbf{y}_1, \mathbf{y}_1, \mathbf{y}_2) = \int \frac{d\Omega(\mathbf{n}_1)}{4\pi} f_0(\mathbf{n}_1, \mathbf{y}_1, \mathbf{y}_2). \quad (47)$$

We use this procedure to evaluate $(V)_1, (V_i)_1$ and their derivatives at the source point. We remark that the regularization procedure should be applied separately on the Riemann tensor and on the orthonormal tetrad. However, at the PN order we are considering, it is perfectly equivalent to apply the regularization procedure directly to the tidal tensor $C_{(i)(j)} = R_{\alpha\beta\gamma\delta} e_{(0)}^\alpha e_{(i)}^\beta e_{(0)}^\gamma e_{(j)}^\delta$.

We now express the point particle positions $\mathbf{y}_{1,2}$ in the system center of mass frame, by the following coordinate transformation [52]

$$y_1^i = \left[\frac{m_2}{m} + \nu \frac{m_1 - m_2}{m} \mathcal{P} \right] r_{12}^i + \mathcal{O}(4), \quad (48)$$

$$y_2^i = \left[-\frac{m_1}{m} + \nu \frac{m_1 - m_2}{m} \mathcal{P} \right] r_{12}^i + \mathcal{O}(4),$$

where

$$\mathcal{P} = \frac{1}{c^2} \left[\frac{v_{12}^2}{2} - \frac{Gm}{2r_{12}} \right] + \mathcal{O}(4). \quad (49)$$

Finally, we express C_j^i in the principal frame using the rotation matrix

$$T = \begin{pmatrix} \cos \psi & \sin \psi & 0 \\ -\sin \psi & \cos \psi & 0 \\ 0 & 0 & 1 \end{pmatrix} \quad (50)$$

where ψ is defined by Eq. (3)

$$\frac{d\psi}{d\tau} = \Omega. \quad (51)$$

The complete form of the tidal tensor $c = TCT^T$ is given by:

$$c_{xx} = -\frac{Gm_2}{2r_{12}^3} \{1 + 3 \cos[2\psi_l]\} + \frac{G}{4c^2 r_{12}^4} \left\{ [6Gm_2^2 + 5Gm\mu + 3\dot{r}_{12}^2 m_1 \nu r_{12}] (1 + 3 \cos[2\psi_l]) - 6\dot{\phi}^2 m_2 r_{12}^3 (1 + \cos[2\psi_l]) + 6m_2 r_{12}^2 \left(\frac{m_2^2}{m^2} + 2\nu \right) \dot{\phi} r_{12} \sin[2\psi_l] \right\} + \frac{3GS_2^z}{mc^3 r_{12}^3} \left\{ \dot{\phi} (m_2 - m_1) + (m_2 - 5m_1) \dot{\phi} \cos[2\psi_l] + \dot{r}_{12} \frac{(m_2 + 3m_1)}{r_{12}} \sin[2\psi_l] \right\} \quad (52)$$

$$c_{yy} = -\frac{Gm_2}{2r_{12}^3} \{1 - 3 \cos[2\psi_l]\} + \frac{G}{4c^2 r_{12}^4} \left\{ [6Gm_2^2 + 5Gm\mu + 3\dot{r}_{12}^2 m_1 \nu r_{12}] (1 - 3 \cos[2\psi_l]) - 6\dot{\phi}^2 m_2 r_{12}^3 (1 - \cos[2\psi_l]) + \right.$$

$$- 6m_2 r_{12}^2 \left(\frac{m_2^2}{m^2} + 2\nu \right) \dot{\phi} r_{12} \sin[2\psi_l] \left\} + \frac{3S_2^z}{mc^3 r_{12}^3} \left\{ \dot{\phi}(m_2 - m_2) - \dot{\phi}(m_2 - 5m_1) \cos[2\psi_l] - \dot{r}_{12} \frac{(m_2 + 3m_1)}{r_{12}} \sin[2\psi_l] \right\} \quad (53)$$

$$c_{zz} = \frac{Gm_2}{r_{12}^3} - \frac{G}{c^2} \left[3 \frac{Gm_2^2}{r_{12}^4} + \frac{5}{2} \frac{Gm\mu}{r_{12}^4} + \frac{3}{2} \frac{m_1 \nu \dot{r}_{12}^2}{r_{12}^3} - \frac{3}{r_{12}} m_2 \dot{\phi}^2 \right] - \frac{6G(m_2 - m_1) S_2^z}{mc^3 r_{12}^3} \dot{\phi} \quad (54)$$

$$c_{xy} = \frac{3Gm_2}{2r_{12}^3} \sin[2\psi_l] + \frac{3G}{4c^2 r_{12}^4} \left\{ 2m_2 r_{12}^2 \left(\frac{m_2^2}{m^2} + 2\nu \right) \dot{\phi} r_{12} \cos[2\psi_l] - \left[6Gm_2^2 + 5Gm\mu + 3\dot{r}_{12}^2 m_1 \nu r_{12} - 2\dot{\phi}^2 m_2 r_{12}^3 \right] \times \right. \\ \left. \times \sin[2\psi_l] \right\} - \frac{3GS_2^z}{mc^3 r_{12}^4} \left\{ \dot{r}_{12} (m_2 + 3m_1) \cos[2\psi_l] + \dot{\phi} (m_2 - 5m_1) r_{12} \sin[2\psi_l] \right\} \quad (55)$$

where the *lag* angle $\psi_l = \psi - \phi + \chi$ describes the misalignment between the axis a_1 and the line between the two objects. In the tidal tensor components the dot indicates differentiation with respect to the coordinate time t . In the principal frame, the geodesic deviation equation for the tidal deformation can be written as

$$\frac{d^2 a_i}{d\tau^2} + c_{ij} a_j = 0. \quad (56)$$

It should be stressed that, as noted in [3], if the system is in quasi-circular inspiral, the radial motion is due only to gravitational back-reaction; consequently $\dot{r}_{12} \simeq (\mathbf{n}_{12} \mathbf{v}_{12}) \sim 1/c^5$ and can be neglected.

3. Comparison with previous expressions of the tidal tensor

As a first check, we compare the tidal tensor derived in [49] for a test particle ($\nu \rightarrow 0$) moving along a geodesic, with our tidal tensor. This tensor has been used in the literature to study tidal effects in binary systems using a quasi-stationary approach [13, 25], or evolving the orbital equations, assuming quasi-circular orbit [31]. Let us consider, as an example, the c_{xx} component for a non-rotating BH. Eq. (70) of ref. [49] gives

$$c_{xx}^{sch} = \frac{Gm_2}{r_s^3} \left(1 - 3 \frac{r_s^2 + K}{r_s^2} \cos[\psi_l]^2 \right), \quad (57)$$

where

$$K = \frac{L_z^2}{c^2} = \frac{1}{c^2} \left(\frac{d\phi}{d\tau} \right)^2 r^4 = \frac{1}{c^2} \left(\frac{d\phi}{dt} \right)^2 r^4 + O\left(\frac{1}{c^4}\right), \quad (58)$$

and r_s is the radial distance in Schwarzschild coordinates. In order to compare Eq. (57) with Eq. (52) we need to express c_{xx}^{sch} in terms of the same radial coordinate adopted for the PN expansion

$$r_s = r_{12} \left(1 + \frac{Gm_2}{2c^2 r_{12}} \right)^2. \quad (59)$$

We find (up to $1/c^3$ terms)

$$c_{xx}^{sch} = -\frac{Gm_2}{2r_{12}^3} (1 + 3 \cos[2\psi_l]) + \frac{3Gm_2}{2c^2 r_{12}^4} \{ Gm_2 +$$

$$+ 3Gm_2 \cos[2\psi_l] - \dot{\phi}^2 r_{12}^3 - \dot{\phi}^2 r_{12}^3 \cos[2\psi_l] \}. \quad (60)$$

This expression coincides with our Eq. (52), in the limit $\nu \rightarrow 0$ and $\dot{r}_{12} \simeq 0$.

We would like to make a further remark about the difference between the tidal tensor (57), derived from the Schwarzschild metric assuming that m_1 follows a time-like geodesic of the Schwarzschild spacetime, and that derived from a two-body post-Newtonian metric. For a particle in circular orbit, the constant K given in Eq. (58) is

$$\frac{K}{r_s^2} = \frac{Gm_2}{r_s c^2 - 3Gm_2}. \quad (61)$$

The former equation diverges for $r_s \rightarrow 3Gm_2/c^2$. This divergence is present also in the tidal tensor components, as shown by Eq. (57), and it may affect the evaluation of tidal effects even if the distance between the interacting bodies is larger than (but close to) $r_s = 3Gm_2/c^2$.

Conversely, as stressed in [3], such divergence does not appear in the PN equations of motion, and consequently the tidal tensor components (52)-(55) are free of this unphysical behaviour.

On the other hand, as $\nu \rightarrow 0$ our approach loses accuracy, since in the test particle limit the PN expansion is poorly convergent [3].

As a second check we compare our tidal tensor with that used in [8], previously derived in [27] up to order $\sim 1/c^2$ with a completely different approach, based on a multipole expansion. Comparing $-G_2^{ij}$ (Eq. (2.2) of [8]) with our tensor C_{ij} , truncated to order $\sim 1/c^2$, we find that (renaming $m_1 \leftrightarrow m_2$) they coincide.

E. Internal dynamics

The internal dynamics of the NS is described using the Hamiltonian approach in the affine approximation [23, 25], recently improved to take into account general relativistic effects [13]:

$$\mathcal{H} = \mathcal{H}_T + \mathcal{H}_I \quad (62)$$

where \mathcal{H}_I describes the NS internal structure, and \mathcal{H}_T describes the tidal interaction. \mathcal{H}_I is obtained directly from the internal Lagrangian \mathcal{L}_I (5). The tidal Hamiltonian \mathcal{H}_T is obtained from the tidal Lagrangian (built up with the coefficients c_{ij} , Eqns. (52)-(54)):

$$\mathcal{L}_T = -\frac{1}{2}c_{ij}I_{ij}, \quad (63)$$

where

$$\mathbf{I} = \hat{\mathcal{M}} \cdot \text{diag} \left(\frac{a_i}{R_{NS}} \right)^2$$

is the inertia tensor of the star in the principal frame.

In deriving the dynamical equations from the Hamiltonian (62), we use the PN time coordinate t , which is related to the proper time of the star center of mass τ by the relation $d\tau = \gamma(t)^{-1}dt$ where the redshift factor $\gamma(t)$ is:

$$\begin{aligned} \gamma(t) = & 1 + \frac{1}{c^2} \left(\frac{m_2^2 v_{12}^2}{m^2} + \frac{Gm_2}{r_{12}} \right) + \\ & + \frac{1}{8c^4 r_{12}^2} \left\{ 4G^2(m_2^2 - 3m\mu) + 4Gr_{12} \left[-m_1 \nu \dot{r}_{12} \right. \right. \\ & + \left. \left. \frac{m_2}{m^3} (4m_1^3 + 11m_1^2 m_2 + 14m_1 m_2^2 + 5m_2^3) v_{12}^2 \right] \right. \\ & \left. + \frac{m_2^2}{m^4} (4m_1^2 - 4m\mu + 3m_2^2) r_{12}^2 v_{12}^4 \right\}. \quad (64) \end{aligned}$$

It should be mentioned that in previous works, where the affine approach including relativistic corrections was used [13, 25, 31], the contribution of the redshift factor was neglected, i.e., it was assumed $t \simeq \tau$.

We also remark that $\mathcal{H}_T \simeq -\mathcal{L}_T$, since \mathcal{L}_T does not depend on the conjugate momenta.

The equations of motion for the variables $q_i = \{\psi, \lambda, a_1, a_2, a_3\}$ and their conjugate momenta $p_i = \{p_\psi, p_\lambda, p_{a_1}, p_{a_2}, p_{a_3}\}$ are:

$$\frac{da_1}{dt} = \frac{R_{NS}}{\gamma(t)} \frac{p_{a_1}}{\hat{\mathcal{M}}} \quad (65)$$

$$\frac{da_2}{dt} = \frac{R_{NS}}{\gamma(t)} \frac{p_{a_2}}{\hat{\mathcal{M}}} \quad (66)$$

$$\frac{da_3}{dt} = \frac{R_{NS}}{\gamma(t)} \frac{p_{a_3}}{\hat{\mathcal{M}}} \quad (67)$$

$$\begin{aligned} \frac{dp_{a_1}}{dt} = & \frac{\hat{\mathcal{M}}}{\gamma(t)} \left[\Lambda^2 + \Omega^2 - 2\frac{a_2}{a_1} \Lambda \Omega + \frac{1}{2} \frac{\hat{\mathcal{V}}}{\hat{\mathcal{M}}} R_{NS}^3 \tilde{A}_1 \right. \\ & \left. + \frac{R_{NS}^2}{\hat{\mathcal{M}}} \frac{\Pi}{a_1^2} - c_{xx} \right] a_1 \quad (68) \end{aligned}$$

$$\begin{aligned} \frac{dp_{a_2}}{dt} = & \frac{\hat{\mathcal{M}}}{\gamma(t)} \left[\Lambda^2 + \Omega^2 - 2\frac{a_1}{a_2} \Lambda \Omega + \frac{1}{2} \frac{\hat{\mathcal{V}}}{\hat{\mathcal{M}}} R_{NS}^3 \tilde{A}_2 \right. \\ & \left. + \frac{R_{NS}^2}{\hat{\mathcal{M}}} \frac{\Pi}{a_2^2} - c_{yy} \right] a_2 \quad (69) \end{aligned}$$

$$\frac{dp_{a_3}}{dt} = \frac{\hat{\mathcal{M}}}{\gamma(t)} \left[\frac{1}{2} \frac{\hat{\mathcal{V}}}{\hat{\mathcal{M}}} R_{NS}^3 \tilde{A}_3 + \frac{R_{NS}^2}{\hat{\mathcal{M}}} \frac{\Pi}{a_3^2} - c_{zz} \right] a_3 \quad (70)$$

$$\frac{d\lambda}{dt} = \frac{\Lambda}{\gamma(t)} \quad (71)$$

$$\frac{dp_\lambda}{dt} = \frac{1}{\gamma(t)} \frac{d\mathcal{C}}{d\tau} = 0 \quad (72)$$

$$\frac{d\psi}{dt} = \frac{\Omega}{\gamma(t)} \quad (73)$$

$$\frac{dp_\psi}{dt} = \frac{1}{\gamma(t)} \frac{dJ^z}{d\tau} = \frac{\hat{\mathcal{M}}}{R_{NS}} \frac{c_{xy}}{\gamma(t)} (a_2^2 - a_1^2), \quad (74)$$

where

$$\tilde{A}_i \equiv \int_0^\infty \frac{du}{(a_i^2 + u) \sqrt{(a_1^2 + u)(a_2^2 + u)(a_3^2 + u)}}, \quad (75)$$

J^z is the NS angular momentum, and \mathcal{C} is the conjugate momentum associated to λ :

$$\begin{aligned} \mathcal{C} = & \frac{\hat{\mathcal{M}}}{R_{NS}^2} [(a_1^2 + a_2^2) \Lambda - 2a_1 a_2 \Omega] \\ J^z = & \frac{\hat{\mathcal{M}}}{R_{NS}^2} [(a_1^2 + a_2^2) \Omega - 2a_1 a_2 \Lambda]. \quad (76) \end{aligned}$$

\mathcal{C} can be interpreted as the circulation of the fluid [25], i.e., the line integral of the four-velocity on a closed worldline enclosing the system. In absence of viscosity, \mathcal{C} is a constant of motion.

It is worth mentioning that, in the spherical configuration ($a_i = R_{NS}$), the integrals (75) can be solved analytically, finding $\tilde{A}_i = 2/(3R_{NS}^3)$; furthermore, the virial theorem (19) implies that $\hat{\mathcal{V}} = -3\hat{\Pi}$. Consequently, in the spherical limit the terms in $\hat{\mathcal{V}}$ and Π in Eqns. (68)-(70) cancel:

$$\left[\frac{1}{2} \frac{\hat{\mathcal{V}}}{\hat{\mathcal{M}}} R_{NS}^3 \tilde{A}_i + \frac{R_{NS}^2}{\hat{\mathcal{M}}} \frac{\Pi}{a_i^2} \right]_{sph} = 0. \quad (77)$$

This property is crucial to ensure a stable evolution. Indeed, the system (65)-(74) admits an equilibrium solution, for which the star is spherical and non-rotating, and the tidal tensor vanishes, only if the property (77) is satisfied. If such solution exists, the tidal deformation induced by the interaction is basically a perturbation of the equilibrium configuration, and the system of equations is well behaved. Conversely, if the cancellation (77) is not exact, the system becomes unstable, because the terms in $\hat{\mathcal{V}}$ and Π are larger than other terms and the equations are non-linear. We remark that the validity of Eq. (77) is guaranteed in our approach, because the virial theorem is satisfied exactly, as discussed in Section II A.

F. Roche lobe and mass shedding

In the next Section we shall compare the results obtained by numerically integrating the equations of motion

(65)-(74) for a BH-NS coalescence, with those published in the literature; we shall evolve the equations up to an orbital separation, r_{shed} , at which mass shedding sets in.

In order to find the value of r_{shed} , we estimate the Roche lobe radius of the NS during the inspiral. It defines the region surrounding the star where a particle of mass $m_0 \ll m_1$ is bounded to the NS gravitational attraction. Following the strategy adopted in [53], we estimate the three-body potential for masses $m_0 \ll m_1 \leq m_2$ (at Newtonian order) for equatorial orbits in the $x-y$ plane:

$$U(x, y) = -\frac{Gm_1}{|\mathbf{x} - \mathbf{y}_1|} - \frac{Gm_2}{|\mathbf{x} - \mathbf{y}_2|} - \frac{1}{2}\omega^2 x^2 \quad (78)$$

where $\mathbf{y}_{1/2}$ are the $m_{1/2}$ displacement vectors, and the last term is the centrifugal contribution with

$$\omega = \sqrt{\frac{G(m_1 + m_2)}{r_{12}^3}}.$$

Since $U(x, y)$ takes its maximum, U_{Rl} , on the surface defining the Roche lobe, we compute numerically $U(x, y)$, finding the Roche lobe on the $x-y$ plane. Mass shedding starts when the star, which is stretched along the direction of the axis a_1 , touches the Roche lobe.

We also determine the location of the 3 PN ICO (Innermost Circular Orbit), r_{ICO} ; to this aim we minimize the total binding energy of the BH-NS system, including the spin contribution [47]. If $r_{shed} > r_{ICO}$, the NS is disrupted before the merger.

It should be noted that the affine approach is intrinsically non-linear, therefore it takes into account non-linear hydrodynamical effects. It also can describe mode oscillations (see, for instance, [26] and, in a similar framework, [54]). However, it does not account for non-linearities in the tidal tensor; since these effects are of the order of $(R_{NS}/r_{12})^5$ [6], which never exceed $\sim 10^{-4}$, they can be safely discarded.

Higher multipoles (octupole, etc.) of the tidal field are also neglected in the affine approach; they are suppressed by a factor $\sim (R_{NS}/r_{12})^2$ [5, 6]; higher PN orders are suppressed by a factor $\sim m/(r_{12}c^2)$. Both these quantities can become as large as ~ 0.15 as $r_{12} \rightarrow r_{shed}$. Therefore, our approach becomes less accurate in the last stages of the inspiral. We plan to improve our model, computing higher PN orders and higher multipole contributions to the tidal field, in future publications.

III. DYNAMICAL TESTS

To validate our approach, we have integrated the dynamical equations (30)-(34) and (65)-(74) to simulate BH-NS binary coalescences. In order to compare our results with the existing literature, we assume that the neutron star is irrotational (i.e., we set $\mathcal{C} = 0$), while the black hole can rotate.

A. Fully relativistic simulations

We compare our results with fully relativistic simulations from three groups, who have kindly shared the required data with us: the Potsdam group [37] (which we denote by AEI); the Urbana group [20] (URB); the Kyoto/Tokyo group [18] (KT). All simulations (including ours) use the same $\Gamma = 2$ polytropic equation of state. The values of the mass ratio $q = m_2/m_1 = M_{BH}/M_{NS}$, of the BH spin parameter $\tilde{a} = a/M_{BH}$, and of the NS compactness $C = M_{NS}/R_{NS}$ are:

1. AEI simulations: $q = 5$, $\tilde{a} = 0$, $C = 0.1, 0.125, 0.15$;
2. URB simulations: $q = 3$, $\tilde{a} = 0, 0.75$, $C = 0.145$;
3. KT simulations: $q = 2, 3$, $\tilde{a} = 0$, $C = 0.145$.

In order to check the validity of our PN formulae, and to determine the time offset t_{off} between our simulations and the fully relativistic simulations, as a preliminary check we compare the orbital motion. It is worth remarking that the time offset is needed to compare our results with the fully relativistic simulations. In particular, it is needed to compare, for each simulation, the time t_{shed} at which our model predicts the onset of mass shedding, with the time at which this occurs in the corresponding fully relativistic simulation. To this aim we follow the strategy adopted in [46]: we demand that the PN and the numerical gravitational wave frequencies agree at some fiducial frequency ω_m , defining t_{off} as the time for which $\dot{\phi}_{PN}(t_{off}) = \omega_m$.

We remark that since the frequency of the $m = 2$ component of the gravitational wave, $\Omega_{GW} = 2\Omega$, is a gauge invariant quantity (see for instance [46, 55, 56] and references therein), it is an appropriate quantity for our comparisons. On the contrary, it is impossible to directly compare the radial coordinates, since the gauge used by fully relativistic simulations is different from our gauge, and furthermore it changes dynamically during the simulation [55]. Note that here m is the harmonic index, not the total mass as in the rest of the paper.

The comparison with the URB and KT data is shown in Fig. 1, where we plot Ω_{GW} versus time (both normalized to the total mass of the binary). Our profiles are indicated in Fig. 1 with a dashed line, which ends at the onset of mass-shedding. The URB and KT profiles are shown by a continuous line.

As expected [46, 55–58], the PN (and EOB) description of the inspiral phase is in good agreement with fully relativistic simulations. The oscillations in the URB, KT curves shown in Fig. 1, are due to the fact that their initial data have a residual eccentricity, while our orbits are quasi-circular. A comparison with the AEI data gives similar results.

In order to assess the accuracy of our evaluation of the onset of mass shedding, we consider the evolution of the NS central density, $\rho_c(t)$, which is a gauge invariant quantity. We compare our profiles, with those evaluated

by the AEI group for the parameters indicated above. The results are shown in Fig. 2, where the AEI profiles are plotted with a solid line, and our data with a dashed line. In the AEI curves, at some point the central density sharply drops down. This signals the transition to a new equilibrium configuration and hence the possible transfer of mass from the star to the black hole. Determining accurately in the numerical simulations when this transfer begins, is not trivial (tiny amounts of matter are lost from the stellar surface already at large separations). However, it is reasonable to assume that the transfer of mass takes place in the transition between the two different values of the central density and therefore in a time interval of 0.75 ms for the $C=0.1$ model or of 0.25 ms for the $C=0.15$ model (clearly, the smaller the compactness the slower the transfer process) [37]. Overall, therefore, we can take the decrease of ρ_c to roughly mark the stage in which the star fills up the Roche lobe. The dashed line for our $\rho_c(t)$ ends at the onset of mass shedding. This occurs just before the steep decrease of the AEI curves, for the models with compactness $C = 0.1, 0.125$. For the case $C = 0.15$, r_{ICO} is reached before mass-shedding sets in; therefore, the dashed line in the bottom panel of Fig. 2 ends at an earlier time with respect to the sharp drop of the solid line. We also note that the values of the central density in our simulations and in AEI's, agree quite well for the models with $C = 0.1$ and $C = 0.125$. For the model with $C = 0.15$, the AEI data show an increase of the central density at earlier times, probably due to spurious numerical effects.

As a further check, we have compared our estimate of the onset of mass shedding with snapshots of the URB and KT simulations. In Fig. 3, we show these snapshots at the time $t = t_{shed}$, which we evaluate for the different models. At that time, in the URB and KT simulations the NS starts showing a cusp, indicating a mass flow. We remark that this kind of comparison should be considered as purely qualitative, since the stellar boundary in the snapshots corresponds to a threshold value of the stellar density, the choice of which is arbitrary.

We would also like to remark that to compare the results of our approach with those of fully relativistic simulations is not an easy task. In particular, a “clean” comparison of the stellar shape deserves further investigations in close interaction with numerical relativity groups, and will be considered in future works.

B. Love number

A different kind of check can be performed by evaluating the Love number which, as discussed in the Introduction, encodes the deformation properties of the star. When a weak tidal field induces a deformation on a spherical star, the star (traceless) quadrupole moment is proportional to the tidal field [6, 7] (see also the generaliza-

tions discussed in [34, 35]):

$$Q_{ij} = -\lambda c_{ij} = -\frac{2}{3}k_2 R_{NS}^5 c_{ij}. \quad (79)$$

Eq. (79) (which is written in the principal frame) is based on the “Love number adiabatic approximation” discussed in Section II A C; since it assumes that the timescale of the orbital evolution (and then of the tidal tensor changes) is much larger than that needed for the star to set into a stationary configuration, this assumption may not be correct in the latest phase of the inspiral; however, it is satisfied when the star and the companion are sufficiently far apart.

In our model, the NS quadrupole moment in the principal frame is

$$Q_{ij} = \frac{\hat{\mathcal{M}}}{R_{NS}^2} (a_i a_j - a^2 \delta_{ij}) \quad (80)$$

where $a^2 \equiv (a_1^2 + a_2^2 + a_3^2)/3$, and c_{ij} is given in Eqns. (52)-(55). In order to compare the Love number k_2 predicted by our approach with those determined by Hinderer [7], which we denote by k_2^H , we have evaluated k_2 using Eqns. (79), (80) for the same NS models, assuming a polytropic equation of state with different values of the adiabatic index Γ and of the compactness C , by setting the binary system at the orbital separation of $r_{12} \sim 180$ km. As shown in Table I, our results agree with those of [7] within a few percent.

We remark that the Love number approach was generalized in [34, 35], where other Love numbers were introduced; however, the leading tidal effect is encoded in k_2 .

C	Γ	k_2	k_2^H
0.10	1.830	0.0920	0.0931
0.15	1.830	0.0551	0.0577
0.20	1.830	0.0297	0.0327
0.10	2.000	0.1221	0.1220
0.15	2.000	0.0767	0.0776
0.20	2.000	0.0444	0.0459
0.10	2.423	0.1817	0.1780
0.15	2.423	0.1198	0.1170
0.20	2.423	0.0737	0.0721

TABLE I. The Love number k_2 , evaluated for different values of the NS compactness C , and of the polytropic index Γ , is compared with the values obtained in [7] for the same stellar models.

IV. CONCLUDING REMARKS

In this article we have developed a post-Newtonian-affine (PNA) approach which allows to model the tidal deformations of a neutron star in compact binary coalescences. To validate the model through a comparison with the results of fully relativistic, numerical simulations, we

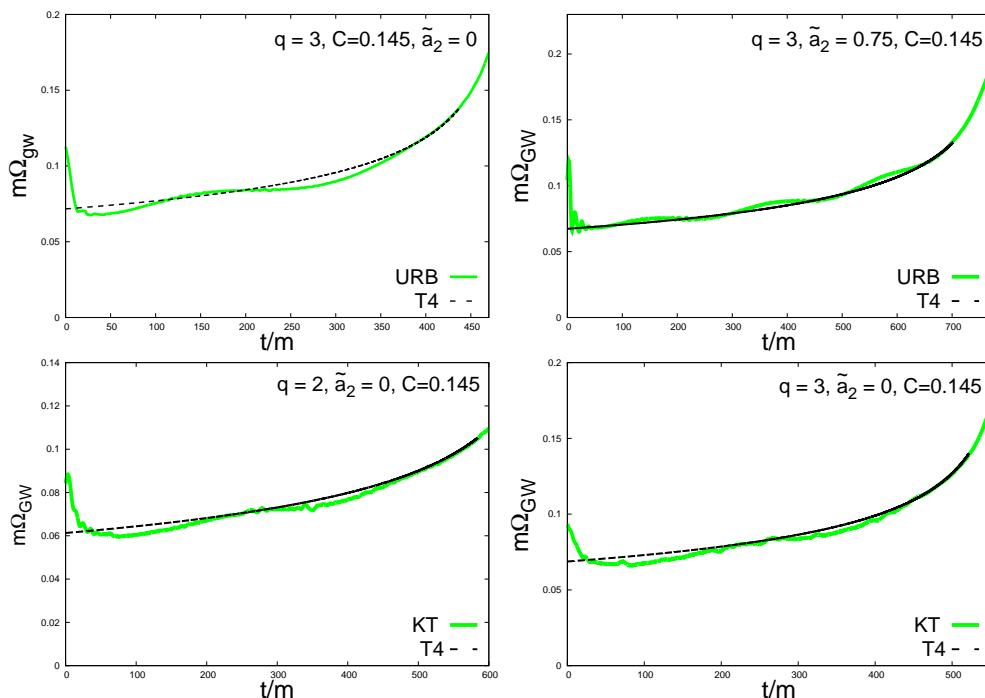


FIG. 1. (Color online) We plot the gravitational wave frequency Ω_{GW} versus time, both normalized to the total mass of the binary. The URB, KT data are indicated by a solid line, and our data by a dashed line. The dashed lines stop at $r_{12} = r_{shed}$, where the deformed star touches the Roche lobe.

have solved the dynamical equations for BH-NS binary systems. The tests we have made show a good agreement with those results.

The PNA approach can be useful in many respects. It may complement numerical relativity studies of binary coalescence because, due to its much lower computational cost, it enables to study a large set of models, exploring a wide range of parameters. Furthermore, like all semi-analytic approaches, it would be helpful to dig the physical features of the process out of the numerical artifacts which may affect the fully relativistic simulations.

Since the PNA approach does not assume the “Love number adiabatic approximation”, it would allow to test the validity domain of this assumption. Indeed, using the PNA framework, it would be possible to determine under which conditions the NS deformation is characterized by a set of constant coefficients, and to find their behaviour, if they change during the inspiral.

Finally, we would like to remind that the production of initial data for fully relativistic simulations is a very delicate task. Typically, initial data are plagued by spurious effects like, for instance, a non-physical eccentricity (compact binaries are known to circularize well ahead the latest stages of the inspiral); it is difficult to produce truly general initial data (for instance, with non-aligned spins). The PNA approach could be used to produce initial data for fully relativistic simulations, complementing existing initial data solvers.

These aspects, and the extension of the PNA approach to the study of NS-NS coalescences, will be the matter of future works.

ACKNOWLEDGMENTS

We thank F. Pannarale, L. Rezzolla, U. Sperhake, Z. Etienne and K. Kyutoku for useful discussions. We thank the Albert Einstein Institute Numerical Relativity Group [37], the Illinois Numerical Relativity Group [20], and the Numerical Relativity Groups of the Kyoto and Tokyo Universities [18], for kindly sharing their data with us. This work was partially supported by CompStar, a research networking program of the European Science Foundation. L.G. has been partially supported by Grant No. PTDC/FIS/098025/2008.

Appendix A: Post-Newtonian expressions for the orbital motion

In this Appendix we write explicitly the post-Newtonian coefficients a_k of the Taylor T4 approximant eq.(30), for spinning bodies in quasi-circular orbits, with spins aligned with the direction of the Newtonian orbital angular momentum vector [45]:

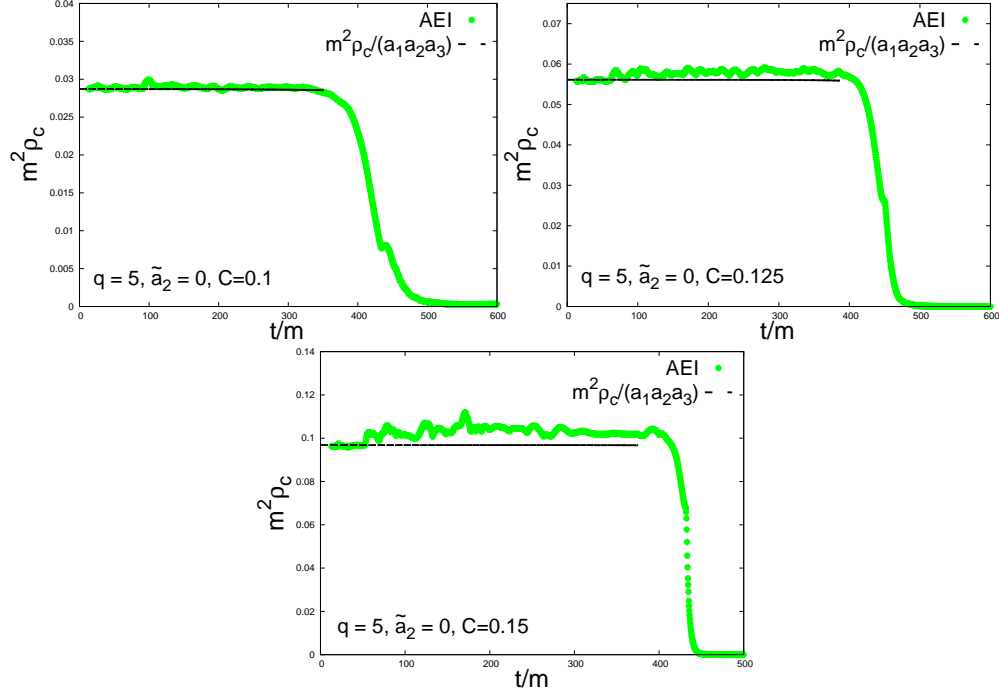


FIG. 2. (Color online) The NS central density (normalized to the squared total mass of the binary) is plotted, as a function of time (normalized to the binary total mass), for the AEI simulations (solid line) and for our simulations (dashed line).

$$\begin{aligned}
a_0 &= 1, & a_1 &= 0, & a_2 &= -\frac{743}{336} - \frac{11\nu}{4}, & a_3 &= 4\pi - \frac{113}{12}\chi + \frac{19\nu}{6}(\tilde{a}_1 + \tilde{a}_2), \\
a_4 &= \frac{34103}{18144} + 5\chi^2 + \nu \left(\frac{13661}{2016} - \frac{\tilde{a}_1\tilde{a}_2}{8} \right) + \frac{59\nu^2}{18}, \\
a_5 &= -\pi \left(\frac{4159}{672} + \frac{189}{8}\nu \right) - \chi \left(\frac{31571}{1008} - \frac{1165}{24}\nu \right) + (\tilde{a}_1 + \tilde{a}_2) \left(\frac{21863}{1008}\nu - \frac{79}{6}\nu^2 \right) - \frac{3}{4}\chi^3 + \frac{9\nu}{4}\chi\tilde{a}_1\tilde{a}_2, \\
a_6 &= \frac{16447322263}{139708800} - \frac{1712}{105}\gamma_E + \frac{16\pi^2}{3} - \frac{856}{105}\ln(16x) + \nu \left(\frac{451\pi^2}{48} - \frac{56198689}{217728} \right) + \frac{541}{896}\nu^2 - \frac{5605}{2592}\nu^3 \\
&\quad - \frac{80\pi}{3}\chi + \left(\frac{20\pi}{3} - \frac{1135}{36}\chi \right) \nu(\tilde{a}_1 + \tilde{a}_2) + \left(\frac{64153}{1008} - \frac{457}{36}\nu \right) \chi^2 - \left(\frac{787}{144}\nu - \frac{3037}{144}\nu^2 \right) \tilde{a}_1\tilde{a}_2, \\
a_7 &= -\pi \left(\frac{4415}{4032} - \frac{358675}{6048}\nu - \frac{91495}{1512}\nu^2 \right) - \chi \left(\frac{2529407}{27216} - \frac{845827}{6048}\nu + \frac{41551}{864}\nu^2 \right) + 12\pi\chi^2 - \chi^3 \left(\frac{1505}{24} + \frac{\nu}{8} \right) \\
&\quad + (\tilde{a}_1 + \tilde{a}_2) \left(\frac{1580239}{54432}\nu - \frac{451597}{6048}\nu^2 + \frac{2045}{432}\nu^3 + \frac{107\nu}{6}\chi^2 - \frac{5\nu^2}{24}\tilde{a}_1\tilde{a}_2 \right) + \chi\tilde{a}_1\tilde{a}_2 \left(\frac{101}{24}\nu + \frac{3}{8}\nu^2 \right)
\end{aligned}$$

Here γ_E is Euler's constant and $\chi = \frac{m_1}{m}\tilde{a}_1 + \frac{m_2}{m}\tilde{a}_2$, with $\tilde{a}_{1,2}$ dimensionless spin parameters defined in section II C.

potentials:

Appendix B: The tidal tensor

We show the non-vanishing components of the tidal tensor C_j^i up to the $1/c^3$ order, as functions of the PN

$$C_{xx} = -\partial_{xx}^2 V^{(0)} + \frac{1}{c^2} \left\{ -4\partial_{xt}^2 V_x^{(0)} + 4v^y \partial_{xx}^2 V_y^{(0)} - 4v^y \partial_{xy}^2 V_x^{(0)} - (\partial_y V^{(0)})^2 - \partial_{xx}^2 V^{(2)} - \left[\partial_{tt}^2 + (v^y)^2 (\partial_{yy}^2 + 2\partial_{xx}^2) + \right. \right.$$

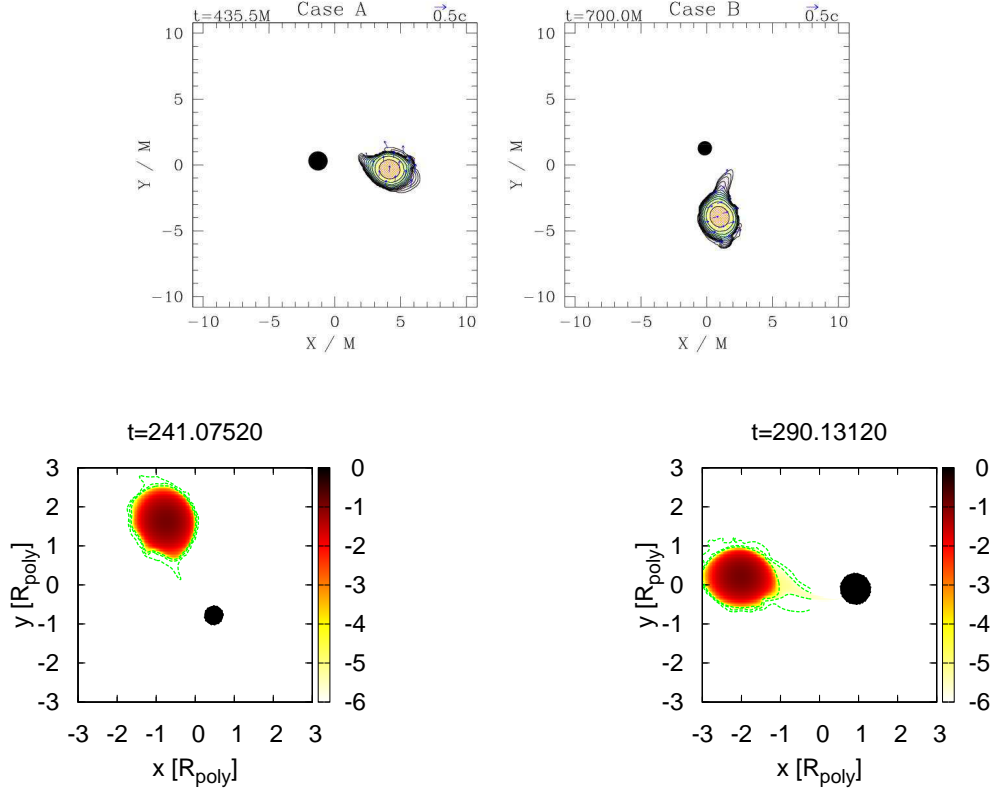


FIG. 3. (Color online) Snapshots corresponding to $t = t_{shed}$ which we evaluate integrating our equations. Upper panels: URB simulations with $C = 0.145$, $\tilde{a} = 0, 0.75$, $q = 3$. Lower panels: KT simulations with $C = 0.145$, $\tilde{a} = 0$, $q = 2, 3$.

$$+ 2v^y \partial_{yt}^2 - v^x v^y \partial_{xy}^2 \left] V^{(0)} + 2\partial_{xx}^2 V^{(0)} V^{(0)} + 2(\partial_x V^{(0)})^2 \right\} - \frac{4}{c^3} \left\{ (\partial_{xt}^2 + v^y \partial_{xy}^2) V_x^{(1)} - v^y \partial_{xx}^2 V_y^{(1)} + \frac{1}{4} \partial_{xx}^2 V^{(3)} \right\}, \quad (B1)$$

$$C_{yy} = -\partial_{yy}^2 V^{(0)} + \frac{1}{c^2} \left\{ -4\partial_{yt}^2 V_y^{(0)} - (\partial_x V^{(0)})^2 + 4v^x \partial_{yy}^2 V_x^{(0)} - 4v^x \partial_{xy}^2 V_y^{(0)} - \partial_{yy}^2 V^{(2)} - \left[\partial_{tt}^2 + (v^x)^2 (\partial_{xx}^2 + 2\partial_{yy}^2) + \right. \right. \\ \left. \left. + 2v^x \partial_{xt}^2 - v^x v^y \partial_{xy}^2 \right] V^{(0)} + 2\partial_{yy}^2 V^{(0)} V^{(0)} + 2(\partial_y V^{(0)})^2 \right\} - \frac{4}{c^3} \left\{ (\partial_{yt}^2 + v^x \partial_{xy}^2) V_y^{(1)} - v^x \partial_{yy}^2 V_x^{(1)} + \frac{1}{4} \partial_{yy}^2 V^{(3)} \right\}, \quad (B2)$$

$$C_{zz} = -\partial_{zz}^2 V^{(0)} + \frac{1}{c^2} \left\{ 4v^y \partial_{zz}^2 V_y^{(0)} + 4v^x \partial_{zz}^2 V_x^{(0)} - \partial_{zz}^2 V^{(2)} - (\partial_x V^{(0)})^2 - (\partial_y V^{(0)})^2 - \left[\partial_{tt}^2 + 2[(v^x)^2 + (v^y)^2] \partial_{zz}^2 + \right. \right. \\ \left. \left. + 2v^x \partial_{xt}^2 + 2v^y \partial_{yt}^2 + (v^x)^2 \partial_{xx}^2 + (v^y)^2 \partial_{yy}^2 + 2v^x v^y \partial_{xy}^2 \right] V^{(0)} + 2\partial_{zz}^2 V^{(0)} V^{(0)} \right\} + \\ + \frac{4}{c^3} \left\{ v^y \partial_{zz}^2 V_y^{(1)} + v^x \partial_{zz}^2 V_x^{(1)} - \frac{1}{4} \partial_{zz}^2 V^{(3)} \right\}, \quad (B3)$$

$$C_{xy} = -\partial_{xy}^2 V^{(0)} + \frac{1}{c^2} \left\{ \left[v^y \partial_{xt}^2 + v^x \partial_{yt}^2 + \frac{3}{2} v^x v^y (\partial_{xx}^2 + \partial_{yy}^2) - \frac{(v^x)^2 + (v^y)^2}{2} \partial_{xy}^2 \right] V^{(0)} + 3\partial_x V^{(0)} \partial_y V^{(0)} + \partial_{xy}^2 V^{(2)} + \right. \\ \left. + 2\partial_{xy}^2 V^{(0)} V^{(0)} + 2(v^x \partial_{xy}^2 - v^y \partial_{yy}^2 - \partial_{yt}^2) V_x^{(0)} + 2(v^y \partial_{xy}^2 - v^x \partial_{xx}^2 - \partial_{xt}^2) V_y^{(0)} \right\} + \\ + \frac{2}{c^3} \left\{ (v^x \partial_{xy}^2 - v^y \partial_{yy}^2 - \partial_{yt}^2) V_x^{(1)} + (v^y \partial_{xy}^2 - v^x \partial_{xx}^2 - \partial_{xt}^2) V_y^{(1)} - \frac{1}{2} \partial_{xy}^2 V^{(3)} \right\}. \quad (B4)$$

-
- [1] <http://www.ego-gw.it>; <http://www.ligo.caltech.edu>.
- [2] R. Narayan, B. Paczynski, and T. Piran, *Astrophys. J. Lett.* **395**, L83 (1992).
- [3] L. Blanchet, *Living Rev. Relativity*, **9**, 4 (2006).
- [4] A. Buonanno, T. Damour, *Phys.Rev. D* **59** (1999) 084006; T. Damour, A. Nagar, *Phys. Rev. D* **79**, 081503 (2009).
- [5] T. Mora, C.M. Will, *Phys. Rev.* **D69**, 104021 (2004).
- [6] E.E. Flanagan, T. Hinderer, *Phys. Rev.* **D77**, 021502 (2008).
- [7] T. Hinderer, *Astrophys. J.* **677**, 1216 (2008); *ibid.*, **697**, 964 (2009).
- [8] J. Vines, E.E. Flanagan, T. Hinderer, *Phys. Rev.* **D83**, 084051 (2011).
- [9] T. Damour, A. Nagar, *Phys.Rev. D* **81** (2010) 084016.
- [10] J. A. Faber, *Class. Quant. Grav.* **26**, 114004 (2009).
- [11] K. Taniguchi, T. W. Baumgarte, J. A. Faber, S. L. Shapiro, *Phys. Rev. D* **75**, 084005 (2007).
- [12] K. Kyutoku, M. Shibata, and K. Taniguchi, *Phys. Rev.* **D79**, 124018 (2009).
- [13] V. Ferrari, L. Gualtieri, F. Pannarale, *Class. Quant. Grav.* **26**, 125004 (2009).
- [14] V. Ferrari, L. Gualtieri, F. Pannarale, *Phys. Rev.* **D81**, 064026 (2010).
- [15] J. A. Faber, T. W. Baumgarte, S. L. Shapiro, K. Taniguchi, F. A. Rasio, *Phys. Rev. D* **73**, 024012 (2006).
- [16] J. A. Faber, T. W. Baumgarte, S. L. Shapiro, K. Taniguchi, *Astrophys. J.* **641**, L93 (2006).
- [17] M. Shibata, K. Uryu, *Class. Quant. Grav.* **24**, S125 (2007).
- [18] M. Shibata, K. Kyutoku, T. Yamamoto, and K. Taniguchi, *Phys. Rev.* **D79**, 044030 (2009).
- [19] K. Kyutoku, M. Shibata, and K. Taniguchi, *Phys. Rev.* **D82**, 044049 (2010); **84** 049902 (2011).
- [20] Z. B. Etienne, Y. T. Liu, S. L. Shapiro, T. W. Baumgarte, *Phys. Rev. D* **79**, 044024 (2009).
- [21] K. Kyutoku, H. Okawa, M. Shibata, and K. Taniguchi, *Phys. Rev.* **D84**, 064018 (2011).
- [22] M. Shibata, K. Taniguchi, *Living Rev. Relativity*, **14**, 6 (2011).
- [23] B. Carter, J.P. Luminet, *Mon. Not. R. Astron. Soc.* **212**, 23 (1985).
- [24] J.P. Luminet, J.A. Marck, *Mon. Not. R. Astron. Soc.* **212**, 57 (1985).
- [25] P. Wiggins, D. Lai, *Astrophys. J.* **532**, 530 (2000).
- [26] C. Casalvieri, V. Ferrari, A. Stavridis, *Mon. Not. R. Astron. Soc.* **365**, 929 (2006).
- [27] T. Damour, M. Soffel, C. Xu, *Phys. Rev.* **D45**, 1017 (1992).
- [28] E. Racine, E.E. Flanagan, *Phys. Rev.* **D71**, 044010 (2005).
- [29] J. Vines, E.E. Flanagan, arXiv:1009.4919
- [30] F. Pannarale, L. Rezzolla, F. Ohme, J. Read, *Phys. Rev.* **D84**, 104017 (2011).
- [31] F. Pannarale, A. Tonita, L. Rezzolla, *Astrophys. J.* **727**, 95 (2011).
- [32] W. Ogawaguchi, Y. Kojima, *Prog. Theor. Phys.* **96**, 901 (1996).
- [33] T. Hinderer, B.D. Lackey, R.N. Lang, J.S. Read, *Phys. Rev.* **D81**, 123016 (2010).
- [34] T. Damour, A. Nagar, *Phys. Rev.* **D80**, 084035 (2009).
- [35] T. Binnington, E. Poisson, *Phys. Rev.* **D80**, 084018 (2009).
- [36] T. Damour, A. Nagar, *Phys. Rev.* **D81**, 084016 (2010).
- [37] L. Rezzolla, F. Pannarale, private communication (2011).
- [38] S. Chandrasekhar *Ellipsoidal Figures of Equilibrium (The Silliman Foundation Lectures)* (Yale University Press, New Haven) (1969).
- [39] S. Chandrasekhar, *Astrophys. J.* **142**, 1488 (1965).
- [40] L. Blanchet, G. Faye, and B. Ponsot, *Phys. Rev.* **D58**, 124002 (1998).
- [41] G. Faye, L. Blanchet, and A. Buonanno, *Phys. Rev.* **D74**, 104033 (2006).
- [42] L. Blanchet, A. Buonanno, and G. Faye, *Phys. Rev.* **D84**, 064041 (2011).
- [43] P.C. Peters, *Phys. Rev.* **136**, B1224 (1964).
- [44] T. Damour, B.R. Iyer, B.S. Sathyaprakash, *Phys.Rev.* **D63** 044023 (2001).
- [45] L. Santamaria et al., *Phys. Rev.* **D82**, 064016 (2010).
- [46] M. Boyle, D.A. Brown, L.E. Kidder, A.H. Mroue, H.P. Pfeiffer, M.A. Scheel, G.B. Cook, S.A. Teukolsky, *Phys. Rev.* **D76**, 124038 (2007).
- [47] Marc Favata, *Phys. Rev. D* **83**, 024027 (1011).
- [48] B. Mashhoon, *Astrophys. J.* **197**, 705 (1975).
- [49] J.-A. Marck, *Proc. Roy. Soc. Lond.* **Q385**, 431, (1983).
- [50] F.A.E. Pirani, *Acta phys.pol.* **15**, 389 (1956).
- [51] T. Fukushima, *Celest. Mech.* **75**, 4461 (1988).
- [52] L. Blanchet, B.R. Iyer, *Class. Quant. Grav.* **20**, 755 (2003).
- [53] V. Ferrari, M. D'Andrea, E. Berti, *Int. J. Mod. Phys.* **D9**, 495 (2000).
- [54] D. Lai, *Mon. Not. R. Astron. Soc.* **270**, 611 (1994).
- [55] M. Hassan, S. Husa, J.A. Gonzalez, U. Sperhake, B. Brügmann, *Phys. Rev.* **D77**, 044020 (2008).
- [56] M. Campanelli, C.O. Lousto, H. Nakano, Y. Zlochower, *Phys. Rev.* **D79**, 084010 (2009).
- [57] B.D. Lackey, K. Kyutoku, M. Shibata, P.B. Brady, J.L. Friedman, arXiv:1109.3402.
- [58] L. Baiotti, T. Damour, B. Giacomazzo, A. Nagar, L. Rezzolla, *Phys.Rev.* **D84** (2011) 024017, *Phys. Rev. Lett.* **105** 261101 (2010).